A New Prototype for Sound Projection

Ben-Daniel Keller[1], Franz Zotter[1,2]
[1] *University of Music and Performing Arts Graz, Austria*
[2] *Institute of Electronic Music and Acoustics, Email: benkeller@gmx.at*

Introduction

Only sources emitting strongly directional sound beams can separately excite the distinct specular wall reflections of a room. If the reflection of a beam was diffuse enough, it would be the origin of a secondary spherical wave at the point of impact, similarly as the diffuse optical reflection utilized for the projection of images on cinema screens.
A musical utilization of specular acoustic reflections was impressively demonstrated in concerts using IEM's Icosahedral loudspeaker (ICO) using third-order spherical harmonic beamforming [1, 2]. Neither has the ICO been exploited for exciting diffuse reflections nor would its directivity be sufficient to produce loud-enough diffuse sound, compared to the direct sound reaching a large audience.
The interesting range of directions for sound projection are limited to the acoustic screen, i.e., the diffusely reflecting wall. According to recent work of Pausch and Pomberger [3, 4], sound hard boundaries can be inserted to narrow down the angular beamforming range and to get an increased spatial definition within.
Pursuing the novel idea of sound projection to a diffusely reflecting acoustic screen, this contribution presents a prototype tailored to the goal. In particular, the design of the layout, the derivation of underlying mathematical functions and their optimal sampling are presented in this work.

Resulting prototype

Our novel loudspeaker array creates highly directive sound radiation on a spherical section. This section is flanked by sound hard boundaries that confine radiation to this angular area. Limiting possible radiation to a spherical section strongly increases the spatial resolution employing the same number of loudspeakers. Fig. 1 shows the functional principle, fig. 2 the design of the sound projector.

Angular projection range

The azimuth and zenith opening angles (φ, ϑ) were chosen to match the typical screening ratio for video projection of $4:3$. Choosing the spherical equator to be equivalent with the lower boundary the array only radiates to a sector on the upper half space. Therefore it is best positioned close to the floor in front of the audience. A reasonable distance to the reflecting wall demands an azimuthal opening angle of about $90°$ which leads to a zenith opening angle of $67.5°$. A big benefit of this design is the reduced complexity of boundary shapes. The lower azimuth boundary is flat, only the upper azimuth boundary is a cone.

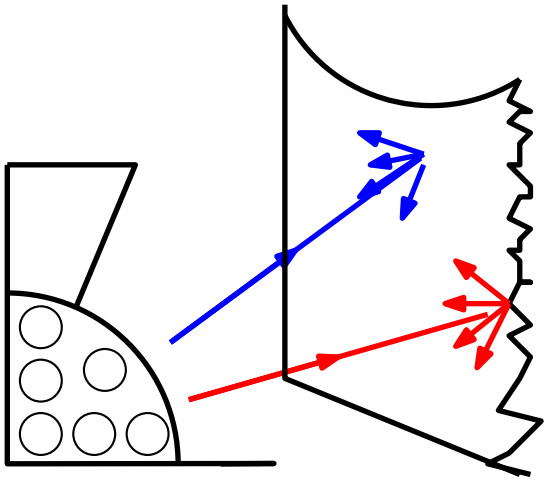

Figure 1: Principle of the sound projector exciting diffuse wall reflections

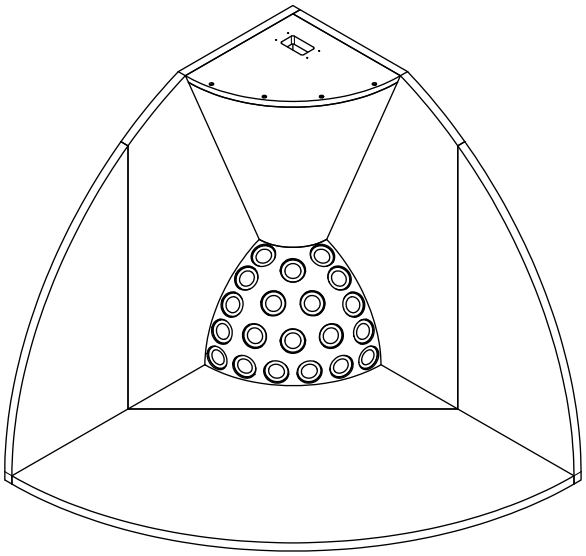

Figure 2: Design of the loudspeaker cabinet

Length of bounding surfaces

Ideally the bounding surfaces should be of infinite length, because they guarantee no radiation of sound beyond them. Obstacles bigger than half of the wavelength λ cause shadowing rather than diffraction ($l_b = \lambda/2$). So the boundary element's length corresponds to the lower frequency boundary for directed sound radiation. Due to transportation issues the length was chosen with $l_b = 550\,\text{mm}$, yielding a *lower frequency boundary* $f_{l,b} = 320\,\text{Hz}$.

Achievable resolution & number of loudspeakers

The upper *frequency limit for spatial aliasing* $f_{u,alias}$ decreases with increasing array radius according to $N > ka$ [5], where N denotes the array's maximum order of modal decomposition , k denotes the wave number and a the array's radius. W.r.t. spatial aliasing a small radius a with a high number of loudspeakers is required. On the other hand, directed radiation and a small array radius requires large membrane excursions at low frequencies. The maximum linear excursion of a loudspeaker becomes the limiting factor here - a larger array radius brings relief. A set of 20 powerful, yet small loudspeakers (membrane diameter = 37 mm) with a maximum linear excursion $x_{max} = \pm 4\,\mathrm{mm}$ were chosen. The array radius was chosen to be as small as possible: $a = 235\,\mathrm{mm}$.

Solution of the Helmholtz equation

The beam pattern of radiation is composed of harmonic functions especially derived for this spherical section. Therefore the Helmholtz equation needs to be solved for the geometry. In spherical coordinates it writes as $(\Delta + k^2)\, p(r, \varphi, \vartheta) = 0$, where Δ is the Laplace operator, $p(r, \varphi, \vartheta)$ is the sound pressure and k is the wave number [5, 6]. It is solved using a product ansatz and separation of variables $p(r, \varphi, \vartheta) = R(r)\Phi(\varphi)\Theta(\vartheta)$. General solutions can be found in [5].

Angular Solutions - Spherical Sector Harmonics

Sound hard bounding surfaces force the perpendicular particle velocity to vanish. Further it is proportional to the derivative of the pressure functions. Physical angular solutions can therefore be found using two-point Neumann boundary conditions. The azimuth Neumann boundary condition writes as $\left.\frac{\mathrm{d}\Phi_\mu(\varphi)}{\mathrm{d}\varphi}\right|_{\varphi_{1,2}} = 0$ and yields the following **azimuth solutions** [4]

$$\Phi_{\mu_m}(\varphi) = N_{\mu_m}\, \cos\left(\mu_m\, \varphi\right), \tag{1}$$

where *degree* $\mu_m = \frac{\pi m}{|\varphi_2 - \varphi_1|}$ for $m = 0, 1, 2, \ldots, \infty$. Note: μ_m is generally of non-integer value. The normalization factor N_{μ_m} is $\sqrt{\frac{2}{|\varphi_2 - \varphi_1|}}$ for $\mu_m \neq 0$ or $\sqrt{\frac{4}{|\varphi_2 - \varphi_1|}}$ for $\mu_m = 0$ to yield an orthonormal basis for $\varphi \in [\varphi_1, \varphi_2]$.

The physical **zenith solution** is a combination of the *associated Legendre functions* of first and second kind $P^{\mu_m}_{\nu_{nm}}$ and $Q^{\mu_m}_{\nu_{nm}}$ with *order* ν_{nm} and *degree* μ_m using two scalar weighting factors α_{nm} and β_{nm} [7].

$$\Theta^{\mu_m}_{\nu_{nm}}(\vartheta) = \alpha_{nm}\, P^{\mu_m}_{\nu_{nm}}(\cos\vartheta) + \beta_{nm}\, Q^{\mu_m}_{\nu_{nm}}(\cos\vartheta), \tag{2}$$

For every μ_m, all corresponding $\nu_{nm} \leq N$, α_{nm}, and β_{nm} fulfilling the Neumann boundary conditions at ϑ_1 and ϑ_2 are calculated numerically using a zero-finding algorithm $\left.\frac{\mathrm{d}\Theta^\mu_\nu(\vartheta)}{\mathrm{d}\vartheta}\right|_{\vartheta_{1,2}} = \left[\alpha\, \frac{\partial P^\mu_\nu(\cos\vartheta)}{\partial\vartheta} + \beta\, \frac{\partial Q^\mu_\nu(\cos\vartheta)}{\partial\vartheta}\right]_{\vartheta_{1,2}} = 0.$
Orthonormality is achieved by suitable scaling of α_{nm} and β_{nm}.

The **Spherical Sector Harmonics** (SSH), as depicted in figure 3, are composed as $Y^m_n(\varphi, \vartheta) = \Theta^{\mu_m}_{\nu_{nm}}(\vartheta)\, \Phi_{\mu_m}(\varphi)$. They form an orthonormal basis on the spherical sector. On the spherical sector, restricted by the boundary, the SSH are orthonormal, i.e.

$$\int_{\varphi_1}^{\varphi_2}\int_{\vartheta_1}^{\vartheta_2} Y^m_n(\varphi, \vartheta) Y^{m'}_{n'}(\varphi, \vartheta)\sin(\vartheta)\,\mathrm{d}\vartheta\,\mathrm{d}\varphi = \delta_{nn'}\delta_{mm'}. \tag{3}$$

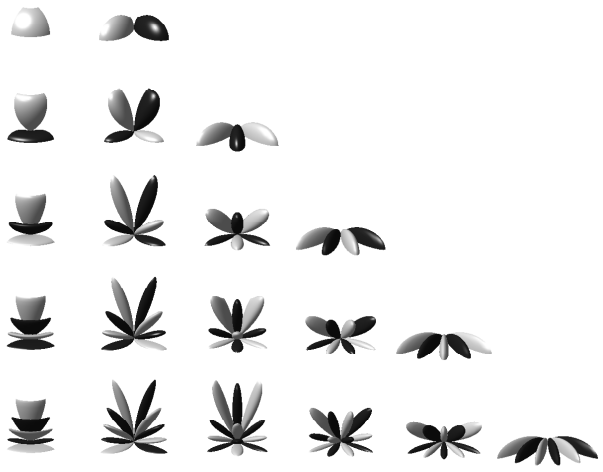

Figure 3: A set of 20 Spherical Sector Harmonics for values μ_m and ν_{nm} fulfilling the arrays geometrical boundary conditions

Radial Solutions

The sound projector is an exterior problem under the simplifying assumption of infinite-length boundaries. As a consequence only the spherical Hankel functions of second kind $h^{(2)}_n$ are solutions to the radial differential equation, [5], the pressure at projection radius r is

$$p(r, \varphi, \vartheta) = \sum_n \sum_m c_{nm}\, h^{(2)}_{\nu_{nm}}(kr)\, Y^m_n(\varphi, \vartheta), \tag{4}$$

where c_{nm} denotes the wave spectra. For large projection radii the far field approximation $\lim_{x\to\infty} h_\nu(x) = j^{\nu+1}\, \frac{e^{-jx}}{x}$ can be used [8], simplifying eq. 4

$$\lim_{r\to\infty} p(r, \varphi, \vartheta) = \sum_n \sum_m c_{nm}\, j^{\nu_{nm}+1}\, \frac{e^{-jkr}}{kr}\, Y^m_n(\varphi, \vartheta). \tag{5}$$

The particle velocity is controlled by the surface of the array at $r = a$, which defines c_{nm}. In SSH it is

$$\zeta_{nm} = \frac{j}{\rho_0 c} c_{nm}\, h'^{(2)}_{\nu_{nm}}(ka)\, Y^m_n(\varphi, \vartheta). \tag{6}$$

So-called radial steering filters $H_{nm}(ka)$ are used to control the particle velocity in order to achieve the desired directivity pattern in the far field ψ_{nm}

$$H_{nm}(ka) = \frac{\rho_0 c}{k}\, \frac{j^\nu}{h'_{\nu_{nm}}(ka)}. \tag{7}$$

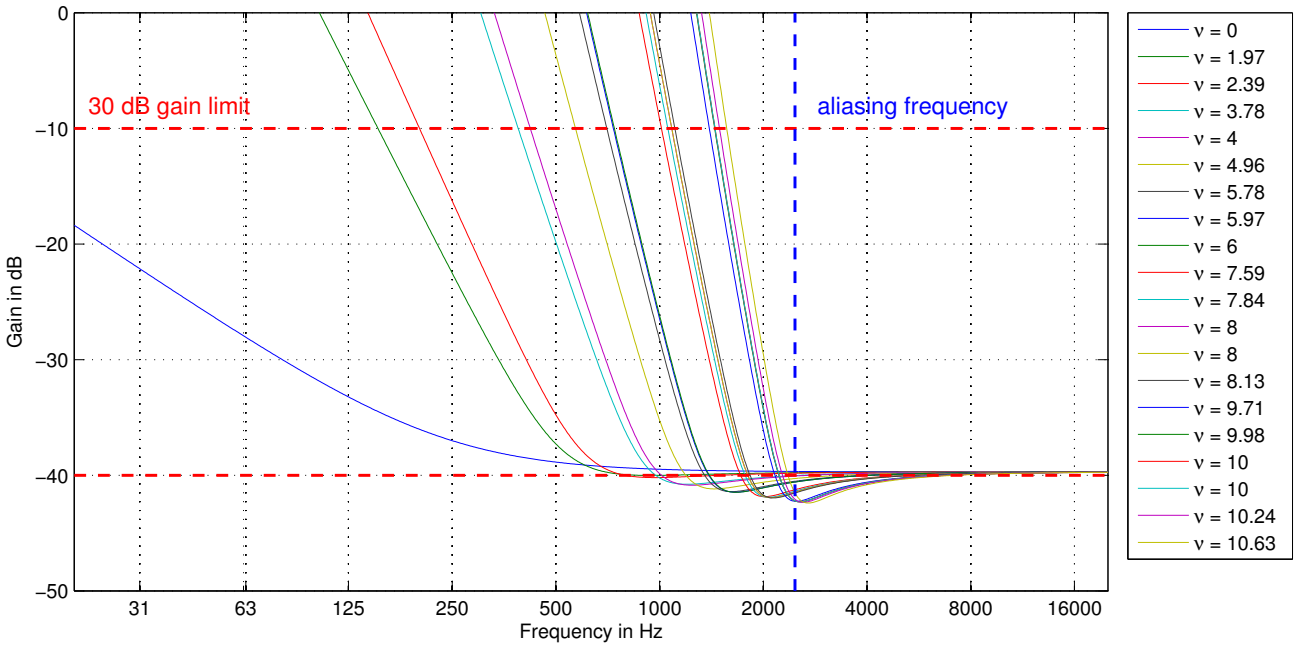

Figure 4: Radial filters for calculated orders ν and radius a, gain limit, upper frequency limit for spatial aliasing

Figure 4 shows the resulting filter weights, a common limit for the gain is 30 dB. The array radius and the maximum spatial resolution of order $N = 10.6$ provide an upper frequency limit for aliasing of $f_{u,alias} = 2.47\,\text{kHz}$. Further, a gain limit of 30 dB has to be introduced due to positioning precision errors and noise (or else small errors are amplified enormously). The gain limit yields lower frequency boundaries for orders ν_{nm}. For example the harmonic of order $\nu_{nm} = 1.97$ can only be used fully for frequencies $f_{low,1.97} > 150\,\text{Hz}$. Below this frequency the order dependent gain has to be limited.

Fig. 5 shows the diagram of signal processing

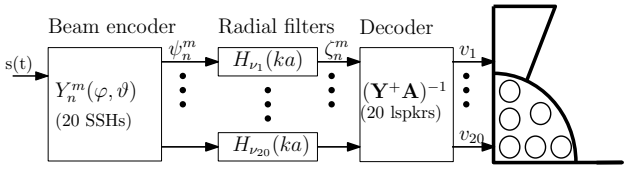

Figure 5: Block diagram of signal flow for modal beamforming

Spherical cap model and layout

For simplicity, driving the array's loudspeakers can be modeled as controlling the membrane velocities. The corresponding surface particle velocity $z(\varphi, \vartheta)$ is described by superimposing cap-shaped aperture functions $a_l(\varphi, \vartheta)$ representing the loudspeaker membranes by 1 inside the l^{th} membrane and 0 elsewhere, cf. [6]:

$$z(\varphi, \vartheta) = \sum_{l=1}^{20} a_l(\varphi, \vartheta)\, v_l. \tag{8}$$

To get the surface velocity in the SSH domain, the equation is transformed. To this end, the 20 aperture functions $a_l(\varphi, \vartheta)$ and the 20 SSH $Y_{nm}(\varphi, \vartheta)$ that should be controlled are sampled by a grid of 22500 HEALPix points [9], yielding the 22500×20 matrices $\boldsymbol{A}$ and $\mathbf{Y}$. We express Eq. (8) discretized, as well as the SSH expansion $z = \sum_{nm} Y_{nm}\, \zeta_{nm}$ as matrix equations

$$\boldsymbol{z} = \boldsymbol{A}\, \boldsymbol{v}, \qquad \boldsymbol{z} = \boldsymbol{Y}\, \boldsymbol{\zeta}. \tag{9}$$

$$\boldsymbol{\zeta} = \boldsymbol{Y}^{-1} \boldsymbol{A}\, \boldsymbol{v}. \tag{10}$$

The sampled cap functions are visualized in figure 6. All spherical cap functions $\mathbf{Y}_{Cap}$, transforming 20 loudspeaker areas to 20 SSH, calculate as

$$\mathbf{Y}_{Cap} = \mathbf{Y}^{-1}\, \mathbf{A}. \tag{11}$$

We assume the loudspeaker's aperture can be approximated by a spatial Dirac δ at its center position. A proof is done via condition number κ after optimizing the center positions via the corresponding SSH transformation matrix $\mathbf{Y}_\delta$.

Optimization

The aim is to sample the sphere such that the transformation matrix $\mathbf{Y}_\delta$ is well conditioned. Approximating a system by considering a wisely chosen subset is a standard procedure in mathematics. The sector is covered with a fine grid of HEALPix points [9]. The SSH transformation matrix is a short-and-fat matrix. Two promising algorithms [10] for the subset selection were examined:

- *Greedy removal*: In each step the column whose deletion yields the lowest condition number is deleted until we end with a square matrix.
- *Greedy selection*: Starting with one suitable column, in each step the one column that yields the lowest

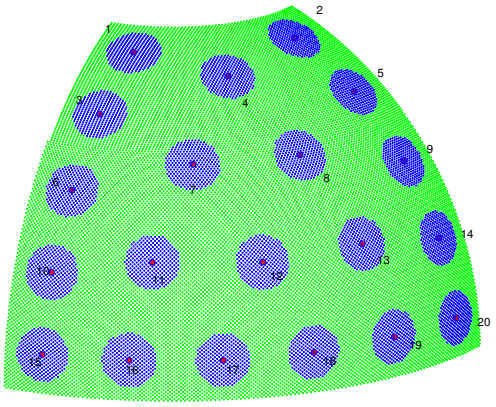

Figure 6: Sampling of the spherical sector, loudspeakers aperture

condition number is added, thus reaching a square matrix.

These algorithm are fast, but there is potential for further optimization: The set of 20 wisely chosen sampling points were fed into MATLAB's unconstrained nonlinear least-squares algorithm optimizing φ and ϑ w.r.t. condition number $\kappa(\mathbf{Y}_\delta)$ simultaneously. The loudspeaker's minimum distance to each other as well as to the border regions were introduced as a strong penalty for κ. The nearly symmetric pattern yielded was manually put into perfect symmetry. The condition number of the transformation matrix is as low as $\kappa(\mathbf{Y}_\delta) = 1.45$. In comparison to critical sampling of a sphere this value is superb. With the positions yielded from optimization the aperture matrix has a condition number of $\kappa(\mathbf{Y}_{Cap}) = 1.6$.

Conclusion and prospects

The equipped prototype is shown in fig. 7.

Figure 7: Sound Projector prototype ready for testing.

Impulse response measurements of every single loudspeakers directivity, similar to [11], will validate the beamforming capability over the frequency spectrum.

Further, membrane velocity measurements using a LASER-Doppler-Vibrometer (LDV) will yield MIMO-equalization filters to flatten the frequency response and cancel speaker cross-talk for each loudspeaker in the shared volume [12].
However, the most interesting question is what kind of wall properties we need for diffuse reflections on a wide frequency range.

References

[1] G. K. Sharma, F. Zotter, and M. Frank, "Orchestrating wall reflections in space by icosahedral loudspeaker: findings from first artistic research exploration," *ICMC-SCM Athens*, 2014.

[2] F. Zotter, M. Frank, A. Fuchs, and D. Rudrich, "Preliminary study on the perception of orientation-changing directional sound sources in rooms," in *Proc. of forum acusticum, Kraków*, 2014.

[3] F. Pausch, "A rigid double cone microphone array prototype," Master's thesis, IEM, 2013.

[4] H. Pomberger and F. Pausch, "Design and evaluation of a spherical segment array with double cone," *Proc. of the EAA Joint Symposium on Auralization and Ambisonics, Berlin, Germany, 3-5 April 2014*, 2014.

[5] E. G. Williams, "Fourier acoustics: Sound radiation and nearfield acoustical holography," 1999.

[6] F. Zotter, *Analysis and Synthesis of Sound-Radiation with Spherical Arrays*. PhD thesis, Kunstuniversität Graz, 2009.

[7] H. Pomberger and F. Zotter, "Modal sound field decomposition applicable for a limited range of directions," *Fortschritte der Akustik, AIA-DAGA, March 2013*, 2013.

[8] M. Pollow and G. K. Behler, "Variable directivity for platonic sound sources based on spherical harmonics optimization," *Acta Acustica united with Acustica*, vol. 95, no. 6, pp. 1082–1092, 2009-11-01T00:00:00.

[9] K. M. Gorski, E. Hivon, A. Banday, B. D. Wandelt, F. K. Hansen, M. Reinecke, and M. Bartelmann, "Healpix: a framework for high-resolution discretization and fast analysis of data distributed on the sphere," *The Astrophysical Journal*, vol. 622, no. 2, p. 759, 2005.

[10] H. Avron and C. Boutsidis, "Faster subset selections for matrices and applications," tech. rep., Cornell University, 2013.

[11] M. Zaunschirm and F. Zotter, "Measurement-based modal beamforming using planar circular microphone arrays," *Proc. of the EAA Joint Symposium on Auralization and Ambisonics, Berlin*, 2014.

[12] H. Pomberger, "Angular and radial directivity control for spherical loudspeaker arrays," Master's thesis, Kunstuniversität Graz, IEM, 2008.